Published in final edited form as:
Structure. 2013 February 5; 21(2): 290–297. doi:10.1016/j.str.2012.12.018.

Deprotonation of D96 in bacteriorhodopsin opens the proton uptake pathway

Ting Wang[1,#], **Ayla O. Sessions**[1,3,#], **Christopher S. Lunde**[1], **Shahab Rouhani**[2], **Robert M. Glaeser**[2], **Yong Duan**[1,*], and **Marc T. Facciotti**[1,*]

[1]Genome Center and Department of Biomedical Engineering, University of California at Davis, One Shields Avenue, Davis, CA 95616, USA

[2]Lawrence Berkeley National Laboratory, Physical Biosciences Division, 1 Cyclotron Road, Berkeley, CA 94720, USA

Summary

Despite extensive investigation, the precise mechanism controlling the opening of the cytoplasmic proton uptake pathway in Bacteriorhodopsin (bR) has remained a mystery. From an analysis of a novel x-ray structure of the D96G/F171C/F219L triple mutant of bR and 60 independent molecular dynamics simulations of bR photointermediates we report that the deprotonation of D96, a key residue in proton transfer reactions, serves two roles that occur sequentially. First, D96 donates a proton to the Schiff-base. Subsequently, the deprotonation of D96 serves to “unlatch” the cytoplasmic side. The latching function of D96 appears to be remarkably robust, functioning to open hydration channels in all photointermediate structures. These results suggest that the protonation state of D96 may be the critical biophysical cue controlling the opening and closing of the cytoplasmic half-channel in bR. We suspect that this protonation-switch mechanism could also be utilized in other proton pumps to minimize backflow and reinforce directionality.

Keywords

bacteriorhodopsin; molecular dynamics; proton pump; conformational change; ion transport; membrane protein; deprotonation

[*]Corresponding Authors: mtfacciotti@ucdavis.edu; Tel: (530)-752-3781; Fax: (530) 754-9658, duan@ucdavis.edu; Tel: (530) 754-5625; Fax: (530) 754-9658.
[3]Present address: Biomedical Sciences Graduate Program, University of California at San Diego, 9500 Gillman Drive, La Jolla, CA 92093, USA
[#]These two authors contributed equally.

Accession Numbers
Atomic coordinates and structure factors for the reported crystal structure have been deposited in the Protein Data Bank under accession number 4PDF.

Supplemental Information
Supplemental Information includes four figures, four tables, and Supplemental Experimental Procedures and can be found with this article online.

Introduction

Bacteriorhodopsin (bR), the heptahelical light-driven proton pump of the archaeon *Halobacterium salinarum*(Lozier et al., 1975), is one of the best-studied membrane proteins and one from which we have derived fundamental knowledge about the ubiquitous process of proton transport. Absorption of an actinic photon isomerizes a lysine-linked retinal chromophore from an *all-trans* to a *13-cis* configuration and triggers a series of conformational changes in the protein that drive a vectorial transfer of a proton from the cytoplasm to the extracellular side of the plasma membrane. During the catalytic photocycle, bR transitions between several discrete intermediate states that can be characterized by time-resolved spectroscopy, termed the K, L, M, N and O states, before returning back to the ground (BR) state (Haupts et al., 1999; Heberle, 2000; Hirai et al., 2009; Lanyi, 2004, 2006). In this study, we highlight how the protonation state of residue D96 mechanistically regulates a key substrate-loading step in the transition between the N and O intermediates.

The structure of bR can be conceptually divided into two functional half-channels that are separated from one another by the retinal: the extracellular (EC) half encompassing the proton release pathway and the cytoplasmic (CP) half comprising the proton uptake pathway. Structural and functional studies have shown that a complex hydrogen-bonded network(Garczarek et al., 2005; Garczarek and Gerwert, 2006; Lorenz-Fonfria et al., 2008; Luecke et al., 1998; Maeda et al., 2006; Mathias and Marx, 2007; Rammelsberg et al., 1998; Wolf et al., 2010), including ionizable residues and water, spans from the Schiff base to the EC surface. Studies have also investigated structural changes occurring during the photocycle, which have the potential to impact the process of proton transfer between the Schiff base and the EC surface (see reviews (Haupts et al., 1999; Hirai et al., 2009)). Despite this abundance of work, only one study explicitly addresses the energetics of proton transfer in the EC half-channel(Braun-Sand et al., 2008). This means that our understanding the relationship between structural changes and of proton transfer itself in the EC half-channel remains incomplete and developing such understanding will require additional experiment and computation.

If the story on the EC side remains incomplete, the CP proton uptake pathway has been even more challenging to characterize owing to the lack of clearly connected sets of ionizable residues between the Schiff base and the cytoplasmic surface and relatively little high-resolution structural information on which to base simulations. An intriguing problem is that one of the few ionizable residues in the CP half channel, D96, lays buried in a hydrophobic environment 12Å from the Schiff base and 7Å from the cytoplasmic surface. Despite its local environs, D96 is known to serve as the key proton donor for the Schiff base(Butt et al., 1989; Gerwert et al., 1989; Holz et al., 1989; Otto et al., 1989; Stern et al., 1989; Tittor et al., 1989) and to be transiently hydrated by the cytosolic water(Cao et al., 1991; Luecke et al., 2000; Luecke et al., 1999; Schatzler et al., 2003; Schobert et al., 2003). For clarity we define the CP half channel as the conducting path extending the entire length from the cytoplasm to the Schiff-base.

The mechanisms by which protons are transferred to and from D96 remain unresolved despite significant inquiry(Cao et al., 1991; Freier et al., 2011; Kandt et al., 2004; Luecke et al., 2000; Luecke et al., 1999; Schatzler et al., 2003; Schobert et al., 2003). Most hypotheses propose that water molecules contribute to the transfer of protons to and from D96 (Cao et al., 1991; Freier et al., 2011; Luecke et al., 2000; Luecke et al., 1999; Schatzler et al., 2003; Schobert et al., 2003). While spectroscopic and neutron scattering experiments(Cao et al., 1991; Maeda et al., 2006; Morgan et al., 2007) suggest that changes in hydration occur during the late phases of the photocycle, the specific role of the water in proton transport (while likely important) remains unconfirmed.

Recently, Freier et al.(Freier et al., 2011) have proposed a model which suggests that a reorganization of internal water molecules, absent any influx of water from the cytosol, may be sufficient to establish a proton conducting path between D96 and the Schiff base. While Freier et al.'s(Freier et al., 2011) discovery sheds new light on the dynamics of internal water molecules, demonstrating that protons explicitly move along this transient path would require additional modeling of the electrostatics(Burykin and Warshel, 2003; Kato et al., 2006). The question of how D96 might be reprotonated during the N-O transition is even less well studied. Like the transfer between D96 and the Schiff base, absence of a clear connection between D96 and the bulk suggests that water might be intimately involved at some point in the reprotonation process. Understanding structural factors altering the reorganization of water in the CP channel is therefore also important.

The reprotonation of the Schiff-base by D96 has traditionally thought to be mediated by, or at least accompanied by, a relatively large structural deformation that begins in the M intermediate and persists through the N intermediate. This structural deformation involves a tilt (outward from the protein axis perpendicular to the membrane plane) of the cytoplasmic ends of helices E, F, and G (Chen and Lanyi, 2009; Haupts et al., 1999; Hirai et al., 2009; Oka et al., 2000; Oka et al., 2002; Vonck, 2000). Additional rearrangements also occur on helix B. The propagation of intramolecular stresses caused by the isomerization of the retinal chromophore is thought to trigger this opening. The role of this tilt in controlling the dynamics of water in the CP channel has not been completely explored.

We sought to investigate this question and other events leading to the opening of the proton uptake channel. We began by solving a 2.65Å x-ray crystallographic structure of the D96G/F171C/F219L triple mutant of bR (crystallization statistics presented in Tables 1 and S1; PDBID 4PDF). The mutant provides a logical starting point for this study, as its ground state is considered analogous to that of the wild-type N intermediate(Subramaniam and Henderson, 2000; Tittor et al., 2002). Due to the highly unstable nature of the detergent solubilized triple mutant protein, crystallization *in meso* was accomplished using a unique formulation of phosphatidylethanolamine-based lipids previously described in detail by Lunde et al(Lunde et al., 2006) (Figure S1).

Results

X-ray crystal structure of bR triple mutant

The identity of the triple mutant was verified by inspecting the structural model and electron density maps (Figure S1). Most of the structural displacements relative to the ground state occur in helices E, F, and G on the cytoplasmic side. The largest of these displacements occurs on Helix F which has an observed average outward tilt of 14.70° ± 1.48°, as measured by the average tilt angle between the α-carbon of the hinge residue P186 and the Cα of residues 164–171 (Figure 1a). The electron density maps in the EF-loop and terminal of helix G regions are shown in Figure S1. This tilt results in a 9.71 Å displacement of the Cα of the helix F residue E166 from its wild-type ground state position (Figure 1b), the largest single displacement. The residues of the E-F loop and the terminus of helix G also show large displacements. For instance, the Cα of S162 on the cytoplasmic end of helix E is displaced by 4.4 Å and beginning at hinge residue 219, helix G tilts towards helix F and the Cα of R227 moves 3.1 Å away from the wild type resting state position. Several rotations around dihedral angles occur between residues 225 and 226 (psi rotates ~78°) and residues 226 and 227 (psi rotates ~ 119°). These rotations, along with other smaller local adjustments result in the movement of the side-chain of R225 from an externally pointing position in the ground state to an internally pointing position in the triple mutant. In addition, these rotations induce a movement of the backbone of helix G towards the position formally occupied by helix F, prior to its outward tilt. Despite the large-scale structural perturbation, a

solvent accessible surface showed that the proton uptake pathway remains functionally closed, terminating on F42. This residue has been previously hypothesized to act as a dynamic gate controlling water and ion flow between the cytosol and the cytoplasmic half-channel(Friedman et al., 2003; Schatzler et al., 2003).

Simulating the N-intermediate

Using 4PFD to further inform our understanding of the reprotonation of D96, we constructed a model analogous to the wild type N intermediate structure by restoring the three mutated residues to their wild-type identities (for a detailed description see Supplemental Experimental Procedures). The resulting model was used as a starting point for 12 molecular dynamics simulations. Nine of these simulations modeled D96 in the deprotonated form while the residue was modeled as protonated in the remaining three. In the three simulations designed to mimic the N-state, the side-chains of D85 and D115 were both protonated and D96 was deprotonated (see Table S3 for pfdND85D115-1, -2, -3). We observed a functional opening occurring either immediately, or within 10 ns of removing restraints on the protein in the simulations with deprotonated D96 (see Movie S1). We characterized a functional opening is by increases in D96-F42 side chain distance, the number and dynamics of water molecules in the D96-K216 cavity, and solvent accessible surface area of D96 (Figure 2). A water channel formed that extended from the cytosol to the Schiff base. The entrance of the channel was lined by the charged residues D38, K41, D102, and R227, previously proposed to act as a proton collecting antenna (Schatzler et al., 2003). The channel narrowed to a bottleneck of 1.24 Å at D96 near a narrow hydrophobic cluster formed by residues F42, L45, L92, L95, L97, L99, L100, and L223 (Figure 3). The bottleneck at D96 is narrowly gated and allows the passage of a single water molecule at a time. The location of the channel gate and its hydrophobic property are in good agreement with the previously proposed “hydrophobic gate” hypothesis(Dencher et al., 1992; Dioumaev et al., 1999; Schatzler et al., 2003). While monitoring water penetration does not give us direct mechanistic insight into the specific mechanism of proton transfer, it is well accepted that the change in hydration of the CP half channel is likely to play a significant role in defining the local environment that otherwise facilitates the process, even if indirectly. Hydration is therefore an important and critical measure of a change in functional state.

Channel opening resulted in minor conformational changes away from the starting model and in highly dynamic exchange of water between the cytoplasm and the open half channel. The conformations of the cytoplasmic ends of helices B, F, and G average a RMSD of 2.20Å relative to the coordinates of the starting structure. The cytoplasmic half channel remained open throughout the simulation, typically filled with 3–4 water molecules. In total 261 different water molecules accessed the D96-K216 cavity during the 87 ns simulation (Figure 3d). These water molecules were highly dynamic and most of them just transiently visited the cavity. Only nine water molecules showed residence time longer than 10 ns. In sharp contrast to the channel opening observed above, when D96 was protonated, the channel remained closed (simulations labeled with green symbols in Figure 2). Throughout these simulations, the protonated D96 was completely buried, as indicated by the small solvent accessible surface area, and the D96-F42 side chain distance remained static. Only either one or two water molecules accessed the D96-K216 in each of these simulations.

To further investigate the functional consequences of D96’s protonation state we also performed a set of similar MD simulations using 1P8U, a model of the N’ state derived from the V49A mutant(Schobert et al., 2003). In these simulations the cytoplasmic half channel functionally opened when D96 was deprotonated and remained closed when D96 was protonated (Figure S2a). In one such simulation the cytoplasmic channel functionally opened at ca. 20 ns and remained open throughout the rest of the simulation. In addition, in

this simulation, the cytoplasmic end of helix F tilted outward from residue V179, adopting a conformation that resembles the more structurally-open states of corresponding residues in 4PFD-based simulations. The cytoplasmic tip of helix B also deformed and swung toward helix A. Despite all of these conformational changes, water exchange with the cytoplasm was nevertheless slower than what was observed in simulations of 4PFD. Fourteen of the 169 water molecules that accessed the D96-K216 cavity stayed longer than 10 ns (Figure S2e), including the four crystal water molecules that stayed longer than 20 ns. Control simulations were conducted by modeling a high salt environment, by restoring V49, and adding the EF-loop missing in the original structure (Figure S2b) and all showed little difference in functional behavior. The inescapable conclusion that emerges from the simulations starting from either the N' or N state structures is that the deprotonation of D96 triggers the functional opening of the cytoplasmic half-channel.

Phenotype robustness and control simulations

We wanted to address whether the D96-linked channel opening was robust to the protonation states of other ionizable sites and other starting structural models. We therefore performed a series of simulations in which the protonation states of other ionizable residues, including D85, D115, E194, and E204, were also varied in the context of eight crystal structures of ground (BR), K, L, M1, M2, N, and N' states (Tables S2 and S3). With D96 as the focus, we made at least two models for each crystal structure: one with deprotonated D96 and the other protonated in which other ionizable side chains (D85, D115, E194, and E204) were set to the state expected in the corresponding photointermediate state. Additional control models and simulations of intermediate states were conducted in which the protonation states of D85, D115, E194, and E204 were again changed.

A consistent picture emerged from these additional simulations. The functional opening of the cytoplasmic half channel was again dependent solely on the protonation state of D96, regardless of the starting structures or the states of other ionizable sites (Figure S3). The number of water molecules that transiently accessed the D96-K216 cavity during the 36 simulations with deprotonated D96 ranged from 20 to 1002 depending on the starting protein conformation (Figure 4 and Table S3). These water molecules are highly dynamic, having a residence time ranging between ~60 ps to ~10 ns. Structural inspection revealed that a stable contiguous chain of water connecting D96 and the Schiff base with the cytoplasm formed in 34 of the 36 simulations (e.g. Movies S2) and the water chain was absent only in two of the 36 simulations. This observation implies that the Schiff base may at some point be directly connected to the cytoplasm, the implications of which are discussed below. Greater conformational flexibility of the cytoplasmic ends of helices B, F and G than the corresponding structures simulated with protonated D96 was also observed (Table S3). This result suggests that the protonation state of D96 has a profound influence on the conformational stability of the helices on the cytoplasmic side of the protein and that this lack of stability can lead to increased hydration of the cytoplasmic half channel. By contrast, when D96 was protonated, the channel remained closed irrespective of the starting structures or the states of other ionizable sites.

Discussion

Despite numerous previous MD simulations on bR, the opening of the proton uptake channel has not been previously reported. This is likely a byproduct of previous MD simulations focusing largely on proton release and the corresponding events occurring in the extracellular half-channel. In the vast majority of these simulations D96 was justifiably modeled in its protonated state(Baudry et al., 2001; Jang et al., 2004; Kandt et al., 2005; Kandt et al., 2004). Even in the very few simulations in which D96 was modeled as deprotonated, the simulations were either very short (1–2.5 ns) (Grudinin et al., 2005; Sato

et al., 2006) or F42 was constrained(Onufriev et al., 2003). The N intermediate was recently simulated based on the N' crystal structure 1P8U and water exchange with the cytoplasm was observed in two of the four 20 ns simulations with deprotonated D96 (Freier et al., 2011). However, the authors focused on reporting the reorganization of internal water molecules involved in the reprotonation of the Schiff base in the cytoplasmic half channel and did not report the extent of water exchange with the cytosol or any evidence of a structural/functional opening of the cytoplasmic half channel. Coincidentally, in our work, the six simulations involving 1P8U in which D96 was deprotonated and D85 and D115 were protonated showed evidence for decreased water exchange with the bulk versus the state in which all three of these residues were deprotonated. The kinetics observed in our simulations (Figure S2) for these six models suggests that the extent of water exchange may have been difficult to appreciate in the previously published 20 ns simulations.

Our simulations indicate that irrespective of starting state, a channel connecting the cytoplasm directly to D96 does not open when D96 is protonated and conversely, when D96 is deprotonated the structure is likely to open (detailed kinetic data is shown in Figure S3). This opening may be mediated by increased conformational flexibility of the ends of helices B, F and G. The deprotonation of D96 appears, however, to be important in latching/unlatching the gate controlling flow of water between the cytoplasm and D96. We therefore posit a mechanism for a two-state model for the N intermediate that could be characterized by structurally distinct states, one corresponding to pre-D96 deprotonation and a second corresponding to post-D96 deprotonation.

In this two-state mechanistic model, the initial deprotonation of the D96 is mediated by a drop in the side chain pKa from >12 in the ground state(Szaraz et al., 1994) to 7.1 in the N state(Dioumaev et al., 2001; Zscherp et al., 1999), likely a consequence of a reorganization of internal water molecules in the space between D96 and the Schiff base and a disruption of the D96-T46 hydrogen bond(Facciotti et al., 2001; Luecke et al., 2000). Our simulations show that when D96 is protonated the D96-T46 hydrogen bond may either remain intact or break depending on the starting protein conformations (Figure S4). Breaking of the D96-T46 hydrogen bond alone is therefore insufficient to open a water-conducting channel in cytoplasmic half channel even in structures that have undergone large conformational changes on the cytoplasmic side. The structural rearrangements associated with the breakage of the D96-T46 hydrogen bond may, however, be sufficient to reorganize internal water molecules between D96 and the Schiff base to facilitate proton transfer (Freier et al., 2011). This is consistent with the two step reprotonation model in which D96 serves as an internal proton donor whose function is pH-independent(Zscherp et al., 1999).

Our simulations suggest that the deprotonation event subsequently "unlatches" the cytoplasmic half-channel thereby establishing a hydration channel (and by consequence a second structural state) that may mediate the reprotonation of D96 from the bulk in a pH-dependent manner, a view consistent with the data and two-step process suggested by Zscherp et al(Zscherp et al., 1999). In this model, the formation of a continuous water channel extending from the Schiff base to the cytoplasm is not a problem provided that the pKa of the Schiff base remains sufficiently higher than pH of the cytoplasm or D96. Since the ground state pKa of the Schiff-base has been reported to be in the neighborhood of 13(Druckmann et al., 1982; Sheves et al., 1986), it not unreasonable to suspect that a dramatic rise in the pKa occurs after reprotonation, perhaps might be mediated by neighboring counterions such as D212. We note explicitly that the above represents a hypothesis drawn from the currently available data. The biophysical role of water in mediating the proton transfer must, however, ultimately rely on electrostatic calculations that use techniques such as Empirical Valence Bond (EVB) treatment, as previously

demonstrated by Warshel and colleagues (Braun-Sand et al., 2008; Kamerlin and Warshel, 2011; Kato et al., 2006).

This work has allowed us to refine our understanding of the N intermediate in bR and the potential role of previously described structural deformations on the cytoplasmic side of the protein. The protonation-state dependent constraint on opening of the cytoplasmic half channel also has functional relevance that may extend to other proton pumps. The concomitant dual role of D96 as both proton donor and "latch" for the cytoplasmic gate and requiring that deprotonation occur prior to unlatching thus helps to determine the directionality of the pump by minimizing the likelihood of backflow.

Methods Summary

Full crystallization, data analysis, and simulation methods and all associated references are presented in the supplemental information. MD simulations were carried out using the AMBER 11 program (Case et al., 2005) and the AMBER ff03 force field (Duan et al., 2003).

Supplementary Material

Refer to Web version on PubMed Central for supplementary material.

Acknowledgments

Mutant membranes were obtained as a kind gift from Drs. Dieter Oesterhelt and Jörg Tittor. This work was supported by the National Institutes of Health (GM67168 to YD), computing resources at the TeraGrid (MCA06N028 to YD and MCB100132 to TW), a UC Discovery Grant (Bio03-10360) to RG, and startup funds to MTF.

References

Baudry J, Tajkhorshid E, Molnar F, Phillips J, Schulten K. Molecular Dynamics Study of Bacteriorhodopsin and the Purple Membrane. J Phy Chem B. 2001; 105:905–918.

Braun-Sand S, Sharma PK, Chu ZT, Pisliakov AV, Warshel A. The energetics of the primary proton transfer in bacteriorhodopsin revisited: It is a sequential light-induced charge separation after all. BBA. Bioenergetics. 2008; 1777:441–452. [PubMed: 18387356]

Burykin A, Warshel A. What really prevents proton transport through aquaporin? Charge self-energy versus proton wire proposals. Biophys J. 2003; 85:3696–3706. [PubMed: 14645061]

Butt HJ, Fendler K, Bamberg E, Tittor J, Oesterhelt D. Aspartic acids 96 and-play a central role in the function of bacteriorhodopsin as a proton pump. EMBO J. 1989; 8:1657–1663. [PubMed: 2548851]

Cao Y, Varo G, Chang M, Ni B, Needleman R, Lanyi JK. Water is required for proton transfer from aspartate-96 to the bacteriorhodopsin Schiff base. Biochemistry. 1991; 30:10972–10979. [PubMed: 1657155]

Case DA, Cheatham TE 3rd, Darden T, Gohlke H, Luo R, Merz KM Jr, Onufriev A, Simmerling C, Wang B, Woods RJ. The Amber biomolecular simulation programs. J Comput Chem. 2005; 26:1668–1688. [PubMed: 16200636]

Chen D, Lanyi JK. Structural changes in the N and N' states of the bacteriorhodopsin photocycle. Biophys J. 2009; 96:2779–2788. [PubMed: 19348761]

Dencher, NA.; Heberle, J.; Buldt, G.; Holtje, HD.; Holtje, M. Active and passive proton transfer steps through bacteriorhodopsin are controlled by a light-triggered hydrophobic gate. In: Rigaud, JL., editor. Structures and Functions of Retinal Proteins. Montrouge: John Libbey Eurotext Ltd; 1992. p. 213-216.

Dioumaev AK, Brown LS, Needleman R, Lanyi JK. Fourier transform infrared spectra of a late intermediate of the bacteriorhodopsin photocycle suggest transient protonation of Asp-212. Biochemistry. 1999; 38:10070–10078. [PubMed: 10433714]

Dioumaev AK, Brown LS, Needleman R, Lanyi JK. Coupling of the reisomerization of the retinal, proton uptake, and reprotonation of Asp-96 in the N photointermediate of bacteriorhodopsin. Biochemistry. 2001; 40:11308–11317. [PubMed: 11560478]

Druckmann S, Ottolenghi M, Pande A, Pande J, Callender RH. Acid-base equilibrium of the Schiff base in bacteriorhodopsin. Biochemistry. 1982; 21:4953–4959. [PubMed: 7138840]

Duan Y, Wu C, Chowdhury S, Lee MC, Xiong G, Zhang W, Yang R, Cieplak P, Luo R, Lee T, et al. A point-charge force field for molecular mechanics simulations of proteins based on condensed-phase quantum mechanical calculations. J Comput Chem. 2003; 24:1999–2012. [PubMed: 14531054]

Facciotti MT, Rouhani S, Burkard FT, Betancourt FM, Downing KH, Rose RB, McDermott G, Glaeser RM. Structure of an early intermediate in the M-state phase of the bacteriorhodopsin photocycle. Biophys J. 2001; 81:3442–3455. [PubMed: 11721006]

Freier E, Wolf S, Gerwert K. Proton transfer via a transient linear water-molecule chain in a membrane protein. Proc Natl Acad Sci U S A. 2011; 108:11435–11439. [PubMed: 21709261]

Friedman R, Nachliel E, Gutman M. The Role of Small Intraprotein Cavities in the Catalytic Cycle of Bacteriorhodopsin. Biophys J. 2003; 85:886–896. [PubMed: 12885636]

Garczarek F, Brown LS, Lanyi JK, Gerwert K. Proton binding within a membrane protein by a protonated water cluster. Proc Natl Acad Sci U S A. 2005; 102:3633–3638. [PubMed: 15738416]

Garczarek F, Gerwert K. Functional waters in intraprotein proton transfer monitored by FTIR difference spectroscopy. Nature. 2006; 439:109–112. [PubMed: 16280982]

Gerwert K, Hess B, Soppa J, Oesterhelt D. Role of aspartate-96 in proton translocation by bacteriorhodopsin. Proc Natl Acad Sci U S A. 1989; 86:4943–4947. [PubMed: 2544884]

Grudinin S, Buldt G, Gordeliy V, Baumgaertner A. Water Molecules and Hydrogen-Bonded Networks in Bacteriorhodopsin--Molecular Dynamics Simulations of the Ground State and the M-Intermediate. Biophys J. 2005; 88:3252–3261. [PubMed: 15731388]

Haupts U, Tittor J, Oesterhelt D. Closing in on bacteriorhodopsin: progress in understanding the molecule. Annu Rev Biophys Biomol Struct. 1999; 28:367–399. [PubMed: 10410806]

Heberle J. Proton transfer reactions across bacteriorhodopsin and along the membrane. BBA. Bioenergetics. 2000; 1458:135–147. [PubMed: 10812029]

Hirai T, Subramaniam S, Lanyi JK. Structural snapshots of conformational changes in a seven-helix membrane protein: lessons from bacteriorhodopsin. Curr Opin Struct Biol. 2009; 19:433–439. [PubMed: 19643594]

Holz M, Drachev LA, Mogi T, Otto H, Kaulen AD, Heyn MP, Skulachev VP, Khorana HG. Replacement of aspartic acid-96 by asparagine in bacteriorhodopsin slows both the decay of the M intermediate and the associated proton movement. Proc Natl Acad Sci U S A. 1989; 86:2167–2171. [PubMed: 2648392]

Jang H, Crozier PS, Stevens MJ, Woolf TB. How Environment Supports a State: Molecular Dynamics Simulations of Two States in Bacteriorhodopsin Suggest Lipid and Water Compensation. Biophys J. 2004; 87:129–145. [PubMed: 15240452]

Kamerlin SCL, Warshel A. The empirical valence bond model: theory and applications. Wiley Interdisciplinary Reviews: Computational Molecular Science. 2011; 1:30–45.

Kandt C, Gerwert K, Schlitter J. Water dynamics simulation as a tool for probing proton transfer pathways in a heptahelical membrane protein. Proteins. 2005; 58:528–537. [PubMed: 15609339]

Kandt C, Schlitter J, Gerwert K. Dynamics of water molecules in the bacteriorhodopsin trimer in explicit lipid/water environment. Biophys J. 2004; 86:705–717. [PubMed: 14747309]

Kato M, Pisliakov AV, Warshel A. The barrier for proton transport in aquaporins as a challenge for electrostatic models: The role of protein relaxation in mutational calculations. Proteins: Structure, Function, and Bioinformatics. 2006; 64:829–844.

Lanyi JK. Bacteriorhodopsin. Annu Rev Physiol. 2004; 66:665–688. [PubMed: 14977418]

Lanyi JK. Proton transfers in the bacteriorhodopsin photocycle. Biochim Biophys Acta. 2006; 1757:1012–1018. [PubMed: 16376293]

Lorenz-Fonfria VA, Furutani Y, Kandori H. Active Internal Waters in the Bacteriorhodopsin Photocycle. A Comparative Study of the L and M Intermediates at Room and Cryogenic Temperatures by Infrared Spectroscopy. Biochemistry. 2008; 47:4071–4081. [PubMed: 18321068]

Lozier RH, Bogomolni RA, Stoeckenius W. Bacteriorhodopsin: a light-driven proton pump in Halobacterium Halobium. Biophys J. 1975; 15:955–962. [PubMed: 1182271]

Luecke H, Richter HT, Lanyi JK. Proton transfer pathways in bacteriorhodopsin at 2.3 angstrom resolution. Science. 1998; 280:1934–1937. [PubMed: 9632391]

Luecke H, Schobert B, Cartailler JP, Richter HT, Rosengarth A, Needleman R, Lanyi JK. Coupling photoisomerization of retinal to directional transport in bacteriorhodopsin. J Mol Biol. 2000; 300:1237–1255. [PubMed: 10903866]

Luecke H, Schobert B, Richter HT, Cartailler JP, Lanyi JK. Structural changes in bacteriorhodopsin during ion transport at 2 angstrom resolution. Science. 1999; 286:255–261. [PubMed: 10514362]

Lunde CS, Rouhani S, Facciotti MT, Glaeser RM. Membrane-protein Stability in a Phospholipid-based Crystallization Medium. J Struct Biol. 2006; 154:223–231. [PubMed: 16600634]

Maeda A, Morgan JE, Gennis RB, Ebrey TG. Water as a cofactor in the unidirectional light-driven proton transfer steps in bacteriorhodopsin. Photochem Photobiol. 2006; 82:1398–1405. [PubMed: 16634652]

Mathias G, Marx D. Structures and spectral signatures of protonated water networks in bacteriorhodopsin. Proc Natl Acad Sci U S A. 2007; 104:6980–6985. [PubMed: 17438299]

Morgan JE, Vakkasoglu AS, Gennis RB, Maeda A. Water structural changes in the L and M photocycle intermediates of bacteriorhodopsin as revealed by time-resolved stepscan Fourier transform infrared (FTIR) spectroscopy. Biochemistry. 2007; 46:2787–2796. [PubMed: 17300175]

Oka T, Yagi N, Fujisawa T, Kamikubo H, Tokunaga F, Kataoka M. Time-resolved x-ray diffraction reveals multiple conformations in the M-N transition of the bacteriorhodopsin photocycle. Proc Natl Acad Sci U S A. 2000; 97:14278–14282. [PubMed: 11106390]

Oka T, Yagi N, Tokunaga F, Kataoka M. Time-resolved X-ray diffraction reveals movement of F helix of D96N bacteriorhodopsin during M-MN transition at neutral pH. Biophys J. 2002; 82:2610–2616. [PubMed: 11964247]

Onufriev A, Smondyrev A, Bashford D. Proton Affinity Changes Driving Unidirectional Proton Transport in the Bacteriorhodopsin Photocycle. J Mol Biol. 2003; 332:1183–1193. [PubMed: 14499620]

Otto H, Marti T, Holz M, Mogi T, Lindau M, Khorana HG, Heyn MP. Aspartic acid-96 is the internal proton donor in the reprotonation of the Schiff base of bacteriorhodopsin. Proc Natl Acad Sci U S A. 1989; 86:9228–9232. [PubMed: 2556706]

Rammelsberg R, Huhn G, Lubben M, Gerwert K. Bacteriorhodopsin's intramolecular proton-release pathway consists of a hydrogen-bonded network. Biochemistry. 1998; 37:5001–5009. [PubMed: 9538019]

Sato Y, Hata M, Neya S, Hoshino T. Computational analysis of the proton translocation from Asp96 to schiff base in bacteriorhodopsin. J Phys Chem B. 2006; 110:22804–22812. [PubMed: 17092031]

Schatzler B, Dencher NA, Tittor J, Oesterhelt D, Yaniv-Checover S, Nachliel E, Gutman M. Subsecond proton-hole propagation in bacteriorhodopsin. Biophys J. 2003; 84:671–686. [PubMed: 12524320]

Schobert B, Brown LS, Lanyi JK. Crystallographic Structures of the M and N Intermediates of Bacteriorhodopsin: Assembly of a Hydrogen-bonded Chain of Water Molecules Between Asp-96 and the Retinal Schiff Base. J Mol Biol. 2003; 330:553–570. [PubMed: 12842471]

Sheves M, Albeck A, Friedman N, Ottolenghi M. Controlling the pKa of the bacteriorhodopsin Schiff base by use of artificial retinal analogues. Proc Natl Acad Sci U S A. 1986; 83:3262–3266. [PubMed: 3458179]

Stern LJ, Ahl PL, Marti T, Mogi T, Dunach M, Berkowitz S, Rothschild KJ, Khorana HG. Substitution of membrane-embedded aspartic acids in bacteriorhodopsin causes specific changes in different steps of the photochemical cycle. Biochemistry. 1989; 28:10035–10042. [PubMed: 2575917]

Subramaniam S, Henderson R. Molecular mechanism of vectorial proton translocation by bacteriorhodopsin. Nature. 2000; 406:653–657. [PubMed: 10949309]

Szaraz S, Oesterhelt D, Ormos P. pH-induced structural changes in bacteriorhodopsin studied by Fourier transform infrared spectroscopy. Biophys J. 1994; 67:1706–1712. [PubMed: 7819502]

Tittor J, Paula S, Subramaniam S, Heberle J, Henderson R, Oesterhelt D. Proton Translocation by Bacteriorhodopsin in the Absence of Substantial Conformational Changes. J Mol Biol. 2002; 319:555–565. [PubMed: 12051928]

Tittor J, Soell C, Oesterhelt D, Butt HJ, Bamberg E. A defective proton pump, point-mutated bacteriorhodopsin Asp96----Asn is fully reactivated by azide. EMBO J. 1989; 8:3477–3482. [PubMed: 2555165]

Vonck J. Structure of the bacteriorhodopsin mutant F219L N intermediate revealed by electron crystallography. EMBO J. 2000; 19:2152–2160. [PubMed: 10811606]

Wolf S, Freier E, Potschies M, Hofmann E, Gerwert K. Directional Proton Transfer in Membrane Proteins Achieved through Protonated Protein-Bound Water Molecules: A Proton Diode. Angew Chem Int Ed Engl. 2010; 49:6889–6893. [PubMed: 20680951]

Zscherp C, Schlesinger R, Tittor J, Oesterhelt D, Heberle J. In situ determination of transient pKa changes of internal amino acids of bacteriorhodopsin by using time-resolved attenuated total reflection Fourier-transform infrared spectroscopy. Proc Natl Acad Sci U S A. 1999; 96:5498–5503. [PubMed: 10318912]

Highlights

- The x-ray crystal structure of the D96G/F171C/F219L of bR is presented.
- MD simulation show that deprotonation of D96 opens the cytoplasmic side.
- Hydration of the cytoplasmic side is influenced by the protonation state of D96.

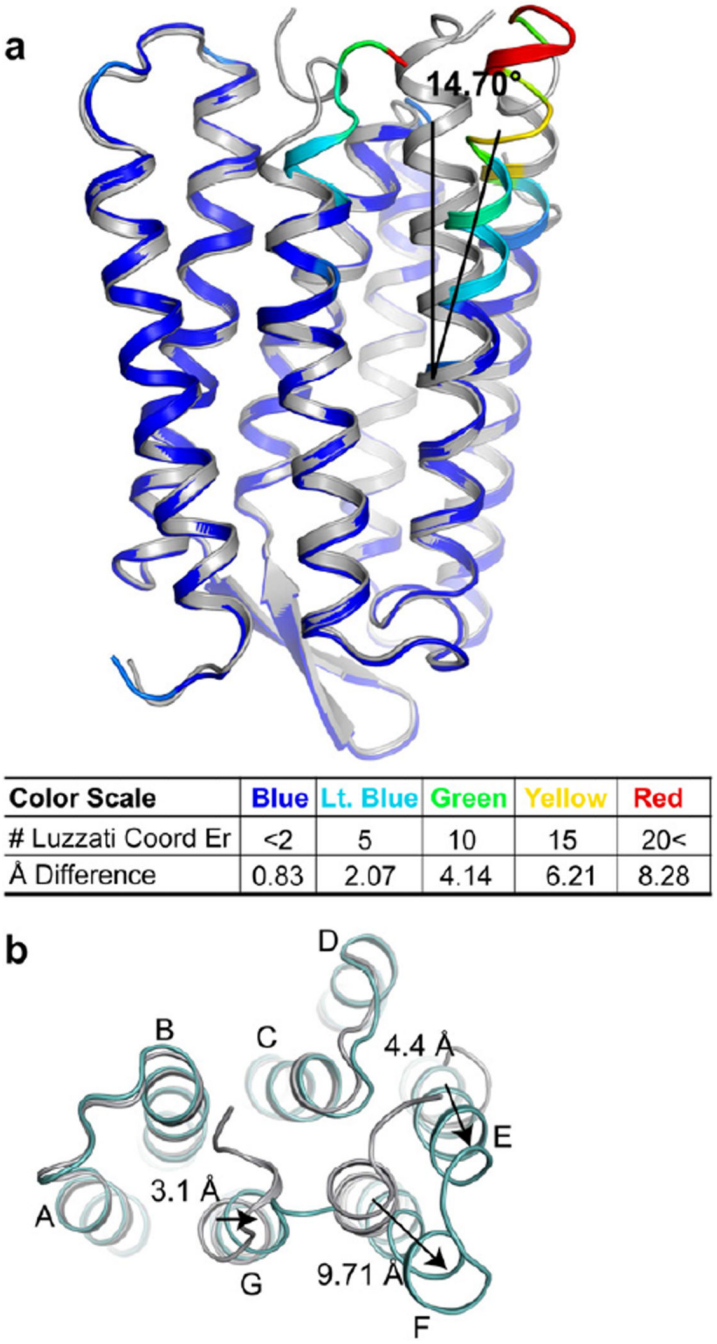

Figure 1. Triple mutant bR structure

Alignments of the triple mutant (colored) to the wild-type ground state structure (silver) are shown along the membrane plane (panel A) and from the cytoplasmic surface. (a) The color scale represents multiples of the Luzzatti coordinate error illustrating significance of conformational change. Helix F tilts outwards from the ground state structure by 14.70° ± 1.48°. (b) Movement of helix F end relative to the ground state as viewed from the cytoplasmic surface. Arrows indicate direction of movement relative to the wild-type ground state starting point. See also Figure S1.

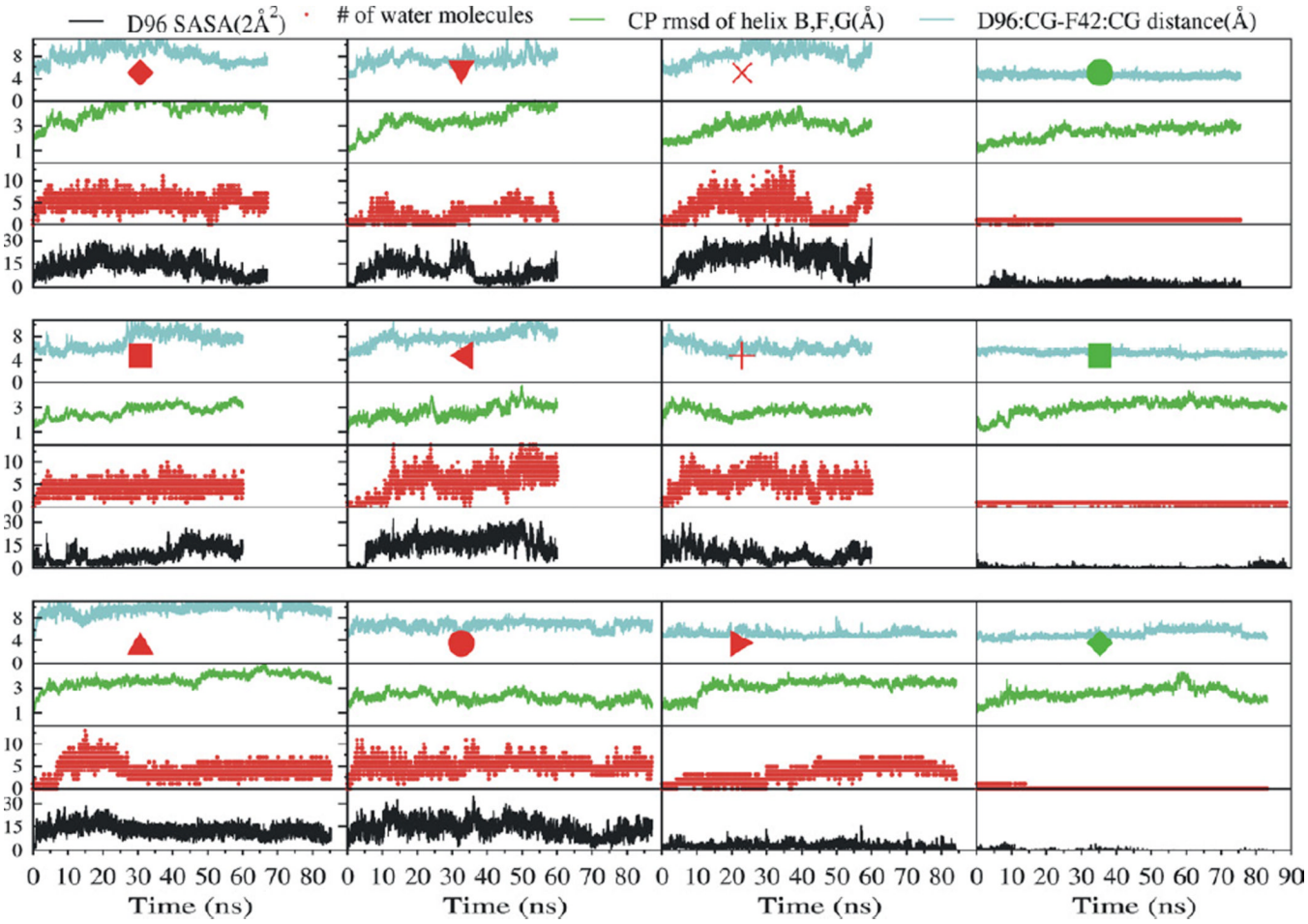

Figure 2. Dynamics in the vicinity of D96 in the simulations based on the triple mutant structure

In each of these simulations the three mutations D96G, F171C, F219L in the crystal structure were modeled back to the wild type. Each box summarizes one metrics measured throughout one complete simulation. For each simulation, the D96-F42 side chain Cγ-Cγ distance (*cyan*), the RMSD of the cytoplasmic ends of helices B, F and G (*green*), the number of water molecules in the D96-K216 cavity (*red*), and the SASA of D96 (*black*), are each plotted against the simulation time. The 9 simulations summarized in the three left-most columns are each labeled by a *red* symbol corresponding to those used in Figure 4 and Table S3. In these simulations D96 is deprotonated. The right-most column shows the results of 3 simulations that are labeled with a *green* symbol corresponding to those used in Figure 4 and Table S3. In these three simulations D96 is protonated.

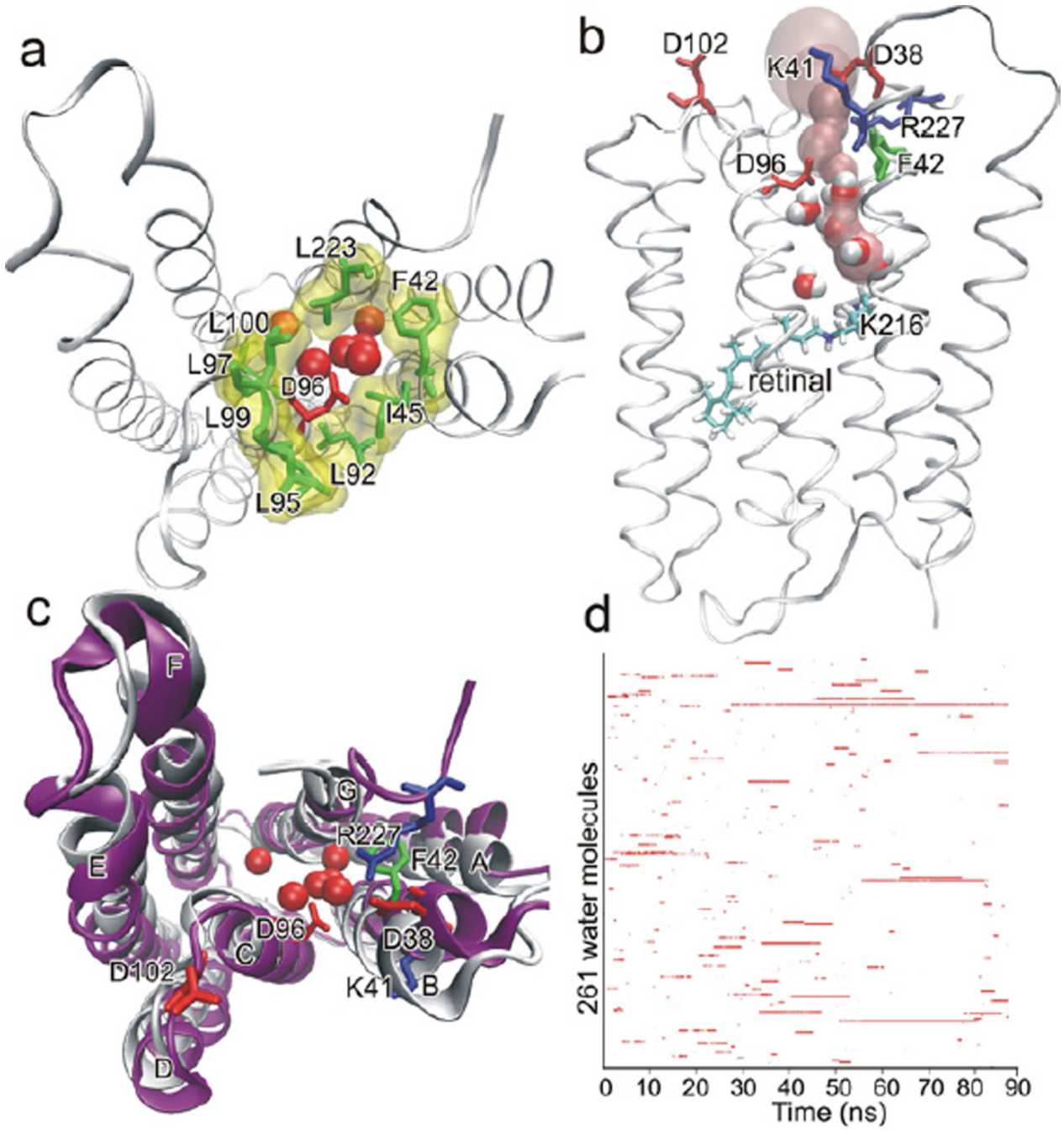

Figure 3. Channel opening in a simulation of an N-state intermediate with deprotonated D96 and protonated D85 and D115

Panels A–C show the last snapshot of the 87 ns simulation pfdND85D115-1 as denoted in Table S3. (a) The model is viewed from cytoplasmic side. Six water molecules are displayed in the D96-K216 cavity (*red ball*). D96 was exposed to the cytoplasmic bulk and surrounded by a hydrophobic cluster formed by F42, L45, L92, L95, L97, L99, L100 and L223 (*green stick and yellow surface*). (b) The pink surface depicts a contiguous water channel, connecting the cytoplasm with K216 and passing by D96. Four water molecules were in the channel, forming a hydrogen-bonded water chain. (c) The helices (*purple*) remained close to the starting conformation (*white*). (d) Binary occurrence of each of the 261 water molecules

that accessed the D96-K216 cavity through the 87 ns simulation. Each row in the y-axis represents a single water molecule. The red line indicates presence and white indicates absence of each respective water molecule in the protein interior. Only nine water molecules had residence time longer than 10 ns. See also Figure S2.

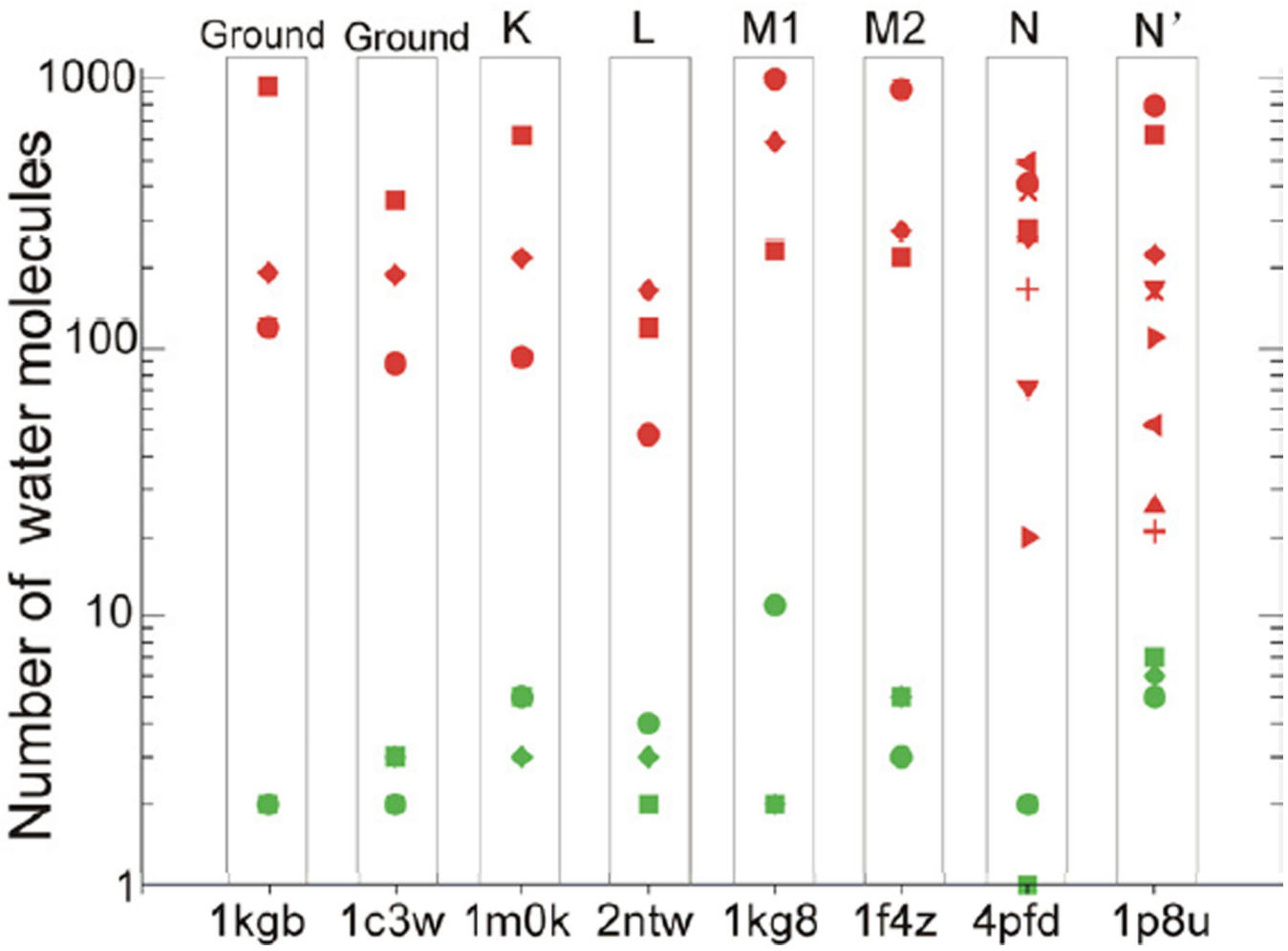

Figure 4. Number of water molecules that accessed the D96-K216 cavity in each of the 60 simulations

Simulations starting from a same crystal structure are boxed in one column. Red symbols represent the simulations in which D96 is deprotonated while green symbols represent the simulations in which D96 is protonated. Each individual simulation is represented with a different shaped symbol, which corresponds directly to the symbols used in Table S3 and reported in Figure 2. The y-axis is $\log_{10}$-scaled. See also Figure S3.

Table 1

Data Collection and Refinement Statistics

Data Reduction and Resolution Range	
Space Group	P6(3)
a, b, c (Å)	60.931, 60.931, 107.701
α, β, γ (°)	90, 90, 120
Data reduction resolution range (Å)/high res.	52.78-2.65/2.82-2.65
Total observations/high res.	41402/4877
Unique structure factors/high res.	6600/928
Average I/σ(I)/high res.	7.8/1/6
Completeness (%)/high res.	99.6/98.1
R_{merge} (%)/high res.	0.208/1.085
Refinement statistics (refinement resolution range 19.25-2.65 Å)	
Twin Ratio	99.5/.5
Number of protein atoms	1738
Number of retinal atoms	20
Number of water molecules	30
Number of lipid atoms	97
R factor (%) for data reso. range/all data	22.5/23.7
R_{free} (%) for data reso. range/all data	25.0/24.0
Average protein B ($Å^2$)	38.9
Average retinal B ($Å^2$)	19.4
Average water B ($Å^2$)	43.2
Average lipid B ($Å^2$)	57.9
Deviation from ideal bond lengths Å	.003
Deviation from ideal bond angles (°)	2.9
Ramachandran Plot Regions (Procheck)	
Favored (%)	91.1
Allowed (%)	98.4
Number of Outliers	0